

Alma Mater Studiorum Università di Bologna
Archivio istituzionale della ricerca

Modelling and field testing of a breakwater-integrated U-OWC wave energy converter with dielectric elastomer generator

This is the final peer-reviewed author's accepted manuscript (postprint) of the following publication:

Published Version:

Moretti G., Malara G., Scialo A., Daniele L., Romolo A., Vertechy R., et al. (2020). Modelling and field testing of a breakwater-integrated U-OWC wave energy converter with dielectric elastomer generator. RENEWABLE ENERGY, 146, 628-642 [10.1016/j.renene.2019.06.077].

Availability:

This version is available at: <https://hdl.handle.net/11585/710428> since: 2019-12-23

Published:

DOI: <http://doi.org/10.1016/j.renene.2019.06.077>

Terms of use:

Some rights reserved. The terms and conditions for the reuse of this version of the manuscript are specified in the publishing policy. For all terms of use and more information see the publisher's website.

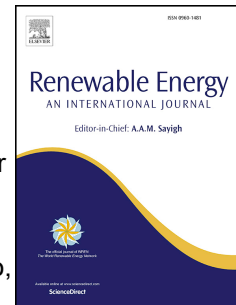
This item was downloaded from IRIS Università di Bologna (<https://cris.unibo.it/>).
When citing, please refer to the published version.

(Article begins on next page)

Accepted Manuscript

Modelling and field testing of a breakwater-integrated U-OWC wave energy converter with dielectric elastomer generator

Giacomo Moretti, Giovanni Malara, Andrea Scialò, Luca Daniele, Alessandra Romolo, Rocco Vertechy, Marco Fontana, Felice Arena



PII: S0960-1481(19)30905-X

DOI: <https://doi.org/10.1016/j.renene.2019.06.077>

Reference: RENE 11809

To appear in: *Renewable Energy*

Received Date: 21 August 2018

Revised Date: 3 June 2019

Accepted Date: 14 June 2019

Please cite this article as: Moretti G, Malara G, Scialò A, Daniele L, Romolo A, Vertechy R, Fontana M, Arena F, Modelling and field testing of a breakwater-integrated U-OWC wave energy converter with dielectric elastomer generator, *Renewable Energy* (2019), doi: <https://doi.org/10.1016/j.renene.2019.06.077>.

This is a PDF file of an unedited manuscript that has been accepted for publication. As a service to our customers we are providing this early version of the manuscript. The manuscript will undergo copyediting, typesetting, and review of the resulting proof before it is published in its final form. Please note that during the production process errors may be discovered which could affect the content, and all legal disclaimers that apply to the journal pertain.

Modelling and field testing of a breakwater-integrated U-OWC wave energy converter with dielectric elastomer generator

Giacomo Moretti^{1,4}, Giovanni Malara², Andrea Scialò², Luca Daniele¹, Alessandra Romolo²,
Rocco Vertechy³, Marco Fontana^{4*}, Felice Arena²

¹TeCIP Institute, Scuola Superiore Sant'Anna, Pisa, Italy

²Natural Ocean Engineering Laboratory (NOEL), "Mediterranea" University of Reggio Calabria, Italy.

³Department of Industrial Engineering, University of Bologna, Italy

⁴Department of Industrial Engineering, University of Trento, Italy

*Corresponding author: marco.fontana-2@unitn.it

Abstract

This paper introduces a theoretical and experimental study of a wave energy converter (WEC) that combines the two innovative concepts of U-oscillating water column (U-OWC) and dielectric elastomer generator (DEG) power take off (PTO). The U-OWC is a type of oscillating water column that features a U-shaped duct that is introduced to tune its dynamics to a certain wave period without active means of phase-control. The DEG is a compliant polymeric generator that makes it possible to convert mechanical energy into electrical energy by exploiting the large deformations of elastomeric membranes.

A lumped-parameter mathematical model of the proposed WEC has been set-up and a small-scale model/prototype has been preliminary tested in a benign real-sea environment. During experiments, relevant experimental data have been collected and used for assessing the reliability of the modelling approach. Beside the model validation, specific experiments have been conducted to test a simple but yet effective load shedding system based on the progressive opening of an air valve. Finally, a preliminary design of a full-scale U-OWC equipped with DEG-PTO has been studied through wave-to-wire analysis. The obtained numerical results show an overall performance that is comparable with that of more conventional, expensive and complex PTO technology.

Keywords: electroactive polymers; system dynamics; resonant systems; oscillating water column; U-OWC; sea test

1. Introduction

Among possible wave energy converter (WEC) architectures, the oscillating water column (OWC) is one of the most investigated both in laboratory and prototypal tests [1]. The OWC is composed by a chamber with a water column that is opened to the wave field in the bottom part and topped by an air chamber in the upper part. In its conventional configuration, the air chamber has an air flow intake (e.g., an orifice) that connects the chamber to a power take-off (PTO) system. The incident waves excite the water column and induce its oscillating motion leading an alternating compression and decompression of the air in the chamber, that in turn produce an air flow through the chamber intake. The mechanical energy of the pressurized air flow is converted by the PTO device into electrical energy.

The OWC and PTO are the key elements of this WEC and they have been deeply investigated in literature [1–4].

Regarding OWCs, several systems have been proposed and developed as stand-alone solutions [5,6], breakwater integrated [7], floating [8] and in arrays [9]. In this context, in the recent years, the concept of U-OWC system has been introduced in [10]. This type of OWC features a narrow vertical U-shaped duct that connects the water column to the open wave field. This element is introduced for tuning the natural period of the water column oscillations with that of the incident waves. It was originally proposed in combination with marine structures for coastal protection. Indeed, it is integrated either in submerged breakwaters or in vertical breakwaters. A direct comparison with a classical OWC showed that it gives better performance in wind-generated seas and in swells because of the mentioned possibility of tuning conveniently its natural period and because of the larger exciting wave pressure amplitudes [11]. The most recent researches on this device provided a theoretical model used for estimating the system response in the time domain, which was validated by small scale

field experiments and a first prototype test used for further validating the model and evaluating the system performance at full scale [12–16].

As regards the PTO, the dominant technologies are the air turbines, such as Wells, impulse turbines, or the recently proposed biradial turbine [17], which share the common feature of rotating always in the same direction irrespective of the air flow direction. These elements were revisited in the last twenty years, in order to improve the efficiency of the whole system, overcome drawbacks of the existing technologies and take advantage of recent new findings.

Recently, dielectric elastomer generators (DEGs) have been proposed as a possible alternative technology for the implementation of PTO [18,19]. DEGs are deformable capacitors based on multifunctional dielectric polymeric materials, referred to as dielectric elastomers (DEs), originally conceived for robotic applications [20,21]. DEGs exploit deformation-driven capacitance variations to perform direct conversion of an input mechanical work into direct-current electrical energy [22]. In the past, DEGs have been implemented according to a diversity of layouts, such as annular membranes subject to out-of-plane deformation [23], inflating diaphragms [24], and tubular membranes [25].

It has been suggested that DEGs can be efficiently employed to harvest energy from different sources, such as human walk, sea currents, and waves [25]. Previous studies indeed demonstrated that DEGs can convert energy densities of up to 780 J/kg (per unit dielectric material mass) [26] and power densities over 200 W/kg at operating frequencies similar to the wave frequencies [24].

Compared to more conventional PTO systems for wave energy harvesting, DEGs are free from rigid/metallic moving parts, they are made of cheap rubber-like materials that are corrosion-resistant and resilient [27,28]. In the past, several DEG PTO implementations for different WEC concepts have been proposed and demonstrated at the scale of laboratory prototype or wave-tank model [18,29–32]. One of the most interesting layouts is the circular

diaphragm DEG (CD-DEG), whose promising performance has been demonstrated by initial theoretical analyses [19] and by further studies on the optimization of the CD-DEG control aimed at maximising the wave power extraction [33]. Furthermore, experimental characterisation of the CD-DEG PTO was accomplished by some of the authors of the present paper through dry-run laboratory tests [34] and wave-tank tests on small-scale OWC prototypes [35], with rated power in the range 1-4 W. Those seminal experiments demonstrated DEGs capability to operate in dynamical conditions in combination with OWCs, converting a significant fraction of the input wave power into electrical power. However, those works were always conducted in controlled laboratory environments and validated against simulated waves. None of the previous works have presented experiments/validations conducted via real sea trials.

In this paper, we present a first set of preliminary real sea-tests based on a comprehensive theoretical investigation/design of a novel WEC that combines an U-OWC system [36] with a set of CD-DEGs as the PTO system. As the first step toward realistic operation at sea, the experiments considered in this article take into account the purely mechanical response of the U-OWC/DEG system, i.e. a passive system that is not include the capability of generating electrical power. The obtained data have been employed to validate a time domain mathematical model of the system response, and they are expected to serve as a basis for future testing. Additionally, a full-scale design for the proposed WEC is presented, which relies on the mechanical model validated in this paper and on experimental outcomes on CD-DEGs power generation obtained in the framework of previous works [35].

The paper is structured as follows. Sect. 2 describes the coupled layout of a U-OWC with a set of CD-DEGs as the PTO and it introduces a mathematical model for the system dynamics. Sect. 3 presents the experimental results and provides a validation of the proposed model.

Sect. 4 proposes and evaluates a concept design of a larger scale U-OWC/DEG wave plant.

Sect 5 finally presents the conclusions.

2. Modeling of U-OWC with DEG PTO.

This section describes the mathematical model of a system composed by a U-OWC caisson embodying a CD-DEG PTO system that is hereafter referred as U-OWC-DEG. First, a general description of the plant is given. Then, the equations of motion of the system are provided.

2.1. U-OWC with DEG PTO: layout and features.

Figure 1 shows a schematic representation of the U-OWC-DEG concept. The system includes a U-OWC caisson that is made of a submerged U-shaped collector that is open to the action of the waves through a horizontal aperture on one side (left side in the picture), and encloses a hollow chamber on the other side. Such a chamber houses an oscillating water column with a volume of air on its top, and presents some circular apertures in the upper walls that make it possible to accommodate the CD-DEGs PTO.

Waves induce an oscillating pressure field on the opening of the U-shaped collector and produce an oscillating motion of the water enclosed in the caisson. As a result, the air volume is subject to fluctuating pressure. Such pressure variation produces the inflation and deflation of the elastomeric membrane (i.e. the variable capacitor) of the CD-DEG that, in combination with a driving power electronics, is responsible of the conversion of mechanical energy into direct current electricity [19] (more details on the working principle and layout are provided in Section 2.2.2).

The U-OWC-DEG system is also equipped with throttle valves in parallel with the CD-DEGs. The valve may be used for preventing overpressures in case of severe sea states.

Relevant geometric parameters are the width of the U-duct and of the OWC collector, respectively, b_1 and b_2 ; the length of the U-duct l_i ; the inlet submergence h_o ; the distance h_c from the top of the air chamber to the mean water level; and the transversal width b_3 .

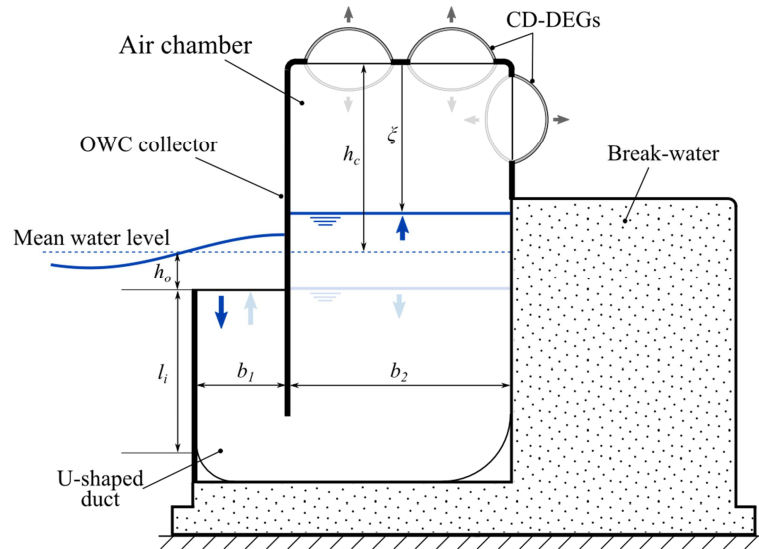


Figure 1. Breakwater integrating a U-OWC with CD-DEGs.

2.2. Mathematical model.

The wave-to-wire model of a U-OWC with DEGs can be regarded as a chain of sub-blocks accounting for different phenomena and/or different portions of the system, namely:

- 1) U-OWC hydrodynamic model, including the wave radiation-diffraction problem, the calculation of the excitation/radiation actions on the U-OWC, and the dynamics of the water column;
- 2) Compressible air chamber response;
- 3) DEG electro-elastic response;

In the following, the models are discussed separately, but it is emphasized that they constitute a coupled system of nonlinear integro-differential equations in the time domain.

2.2.1. U-OWC hydrodynamic model.

The U-OWC water column oscillations are described in time domain by the unsteady Bernoulli equation. The equation is derived by calculating the total head at the water column inlet and the total head at the free surface of the inner water column. The unknown water column displacement ξ is the distance from the top of the air chamber to the inner free surface. Since energy losses along the water column and the U-duct are significant, head losses are included in the model via the instantaneous acceleration-based method, which accounts for steady head losses through a drag-type non-linearity and for unsteady head losses through an inertial term. Both quantities are proportional to constants determined in experimental tests [13,15].

The resulting water column equation of motion is as follows:

$$M(\xi)\ddot{\xi} + C(\xi, \dot{\xi})\dot{\xi} + (\xi - h_c) - \frac{p}{\rho g} - \frac{1}{g} \frac{b_2}{b_1} \int_0^\tau \dot{\xi}(\tau) K(\tau - \theta) d\theta = -\frac{\Delta p^{(D)}}{\rho g}, \quad (1)$$

where τ is the time; g is the acceleration of gravity; ρ is the water density; p is the relative pressure in the air chamber; $M(\xi)$ and $C(\xi, \dot{\xi})$ are, respectively, time-dependent mass and damping terms; $K(\tau)$ is a convolution term which accounts for wave radiation loads; and $\Delta p^{(D)}$ is the wave excitation pressure.

The mass and damping terms read as follow:

$$M(\xi) = \frac{1+C_{in}}{g} \left[\frac{b_2}{b_1} l_i + l_i + h_o + h_c - \xi \right] - \frac{b_2}{g b_1} H(\infty) \quad (2)$$

and

$$C(\xi, \dot{\xi}) = \frac{1}{2g} \left\{ C_{dg} \left[\frac{l_i}{R_{h1}} \left(\frac{b_2}{b_1} \right)^2 + \frac{l_i + h_o + h_c - \xi}{R_{h2}} \right] + 1 \right\} |\dot{\xi}| \quad (3)$$

where $H(\infty)$ is an equivalent length accounting for the infinite frequency added mass, C_{in} and C_{dg} are coefficients accounting for the U-duct head losses, and R_{h1} , R_{h2} are hydraulic radii of the U-duct and inner chamber horizontal sections.

In the previous set of equations, the wave pressure at the inlet section has been taken into account by utilizing Cummins' representation of the radiated wave field under the assumption that the surrounding wave field can be described by potential theory [38,39]. In particular, the total wave pressure has been regarded as the sum of two contributions: 1) the excitation pressure $\Delta p^{(D)}$ representing the wave pressure in a diffractive wave field; 2) and a second contribution related to the wave field radiated by the U-OWC. This second contribution further comprises two terms: a term accounting for the effect of infinite-frequency added mass, $H(\infty)$ (included in the definition of $M(\xi)$), and a convolution integral accounting for the hydrodynamic memory effects. Both $H(\infty)$ and the kernel of the convolution integral $K(\tau)$ are geometric dependent parameters determined by solving pertinent boundary value problems (see [14]).

2.2.2. DEG electro-mechanical model

The CD-DEG is an electrostatic generator that is able to convert the pneumatic work done by a pressure differential applied on its faces into electrical energy. The CD-DEG is a variable electrostatic capacitor shaped as a circular membrane. The applied pressure induces out-of-plane deformations of the membrane resulting in capacitance variations. The CD-DEG membrane is generally implemented as a stack of circular layers of DE and electrodes arranged to form a multilayer capacitor, as shown in Figure 2. Materials commonly used for the DE membranes are acrylics, natural and styrene-based rubber and silicones, which combine the electrical properties of large dielectric breakdown fields and low-conductivity with mechanical properties of large extensibility and reduced stiffness. Compliant electrodes are made of layers of electrically conductive materials that have to maintain low-resistivity even under large stretches. Compliant electrodes are usually implemented as thin metallic films sputtered on the DE substrates or carbon-loaded conductive elastomeric films [37].

In terms of the constitutive model, the DE material can be described as a non-linear hyperelastic continuum (i.e., an elastic solid with non-linear stress-strain response) [40] with dielectric behaviour. Modelling the CD-DEG using local continuum electro-elastic formulations [41] is rather complex and computationally expensive. In order to provide a practical formulation, suitable for design and preliminary analysis, a reduced lumped-parameter model is provided in [19]. In this work, we use a further reduced model, as presented in [18]. The model exploits some simplifying assumptions, previously validated [18,33] and shortly recalled in the following.

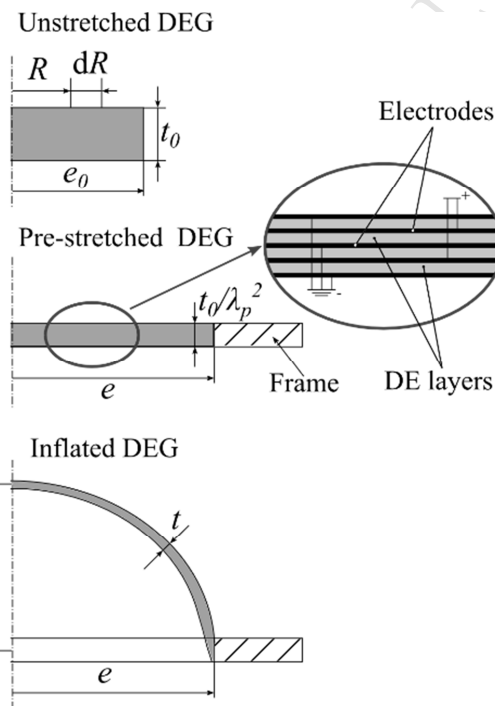


Figure 2. Schematic view of a CD-DEG in its undeformed state (top), pre-stretched mounting configuration (centre) and inflated configuration (bottom). The inset shows the detail of the dielectric-electrode layers.

The geometry of the CD-DEG stack is schematically described in Figure 2. The symbols e_0 and t_0 denote the stack radius and total thickness in the undeformed state. The DEG is

mounted on the holding frame with a certain pre-stretch, λ_p , which takes its radius to $e = \lambda_p e_0$. Rubber-like materials are incompressible (their volume does not change after deformation), therefore, the CD-DEG diameter after pre-stretching is t_0/λ_p^2 . Upon application of a pressure difference p between the DEG lower and upper faces, the latter displaces from the flat equilibrium configuration and undergoes out-of-plane expansion.

As demonstrated in [18], the equilibrium pressure p associated to a given geometric configuration and a voltage difference V applied on the DE layers has the following expression:

$$p = \frac{dU_m}{d\Omega_c} - \frac{V^2}{2} \frac{dC}{d\Omega_c}, \quad (4)$$

where U_m is the elastic energy of the DE layers, Ω_c is the volume subtended by the deformed CD-DEG shell, and C is its capacitance.

Consistently with the assumptions presented in [19], the deformed CD-DEG is approximated as a thin spherical shell with non-uniform thickness. Therefore, its configuration can be uniquely identified by the displacement h_t of the tip element from the equilibrium plane (positive upwards).

Using the assumption of spherical deformation, Ω_c relates to h_t as follows:

$$\Omega_c = \frac{\pi}{6} h_t (h_t^2 + 3e^2), \quad (5)$$

It is also assumed that the deformation state is completely equibiaxial (i.e., the stretch is the same in any direction tangent to the shell surface), though it is not uniform over the DEG. In [19], it has been shown that this assumption provides a good agreement with finite-element simulations in a wide range of DEG deformations, comprised at least between $h_t = -e$ and $h_t = e$. The tangential stretch in a generic point of the DEG reads as follows:

$$\lambda = e e_0 \frac{h_t^2 + e^2}{e^2 e_0^2 + h_t^2 R^2}, \quad (6)$$

where R identifies a material element lying at a distance R from the axis in the unstretched state (see Figure 2). Notice that, owing to incompressibility, the thickness in a generic point of the deformed CD-DEG shell is given by $t = t_0/\lambda^2$.

The deformed CD-DEG layers are parallel-plate capacitors, with total capacitance given by the following expression:

$$C = \frac{\pi \epsilon n_l^2 \lambda_p^2 e^2}{3t_0} \left[\left(\frac{h_t^2 + e^2}{e^2} \right)^3 + \left(\frac{h_t^2 + e^2}{e^2} \right)^2 + \left(\frac{h_t^2 + e^2}{e^2} \right) \right], \quad (7)$$

where ϵ is the DE material dielectric constant, and n_l is the number of dielectric layers in the stack. The total thickness of the dielectric layers is assumed equal to the total DEG thickness, t_0 , being the electrodes thickness negligible.

The DEG elastic energy is a function of the stretch. Modelling the DE material as hyperelastic, the volumetric elastic energy density is given by a strain-energy function, Ψ , whose dependence on λ is expressed by a given constitutive model. The Mooney-Rivlin hyperelastic model [40] is used under the assumption of incompressible solid with equibiaxial deformation. The following expression holds for Ψ :

$$\Psi = C_{1,0}(2\lambda^2 - \lambda^{-4}) + C_{0,1}(2\lambda^{-2} + \lambda^4), \quad (8)$$

where $C_{1,0}$ and $C_{0,1}$ are characteristic constitutive parameters. The total elastic energy, U_m , is the result of the integration of Ψ over the total elastomeric volume:

$$U_m = 2\pi t_0 \int_0^{e_0} R \Psi \, dR. \quad (9)$$

It is worth noticing that the calculation of the derivatives in Eq. (4) can be performed using the chain rule, considering that U_m , Ω_c and C are functions of h_t .

Eq. (4) does not keep into account the mechanical inertia/kinetic energy of the DE material. As observed in [33], the DEG dynamics is expected to be much faster than that of an OWC (i.e., its natural frequency is much larger), thus, for the aim of this paper, the DEG response can be assumed quasi-static.

260 The electric field in the DE layers is given by

$$261 \quad E = n_l \lambda^2 V / t_0, \quad (10)$$

262 and, since it depends on λ , it is not uniform throughout the CD-DEG.

263 The instantaneous electrical power output of the DEG is given by:

$$264 \quad P_u = -V\dot{Q}, \quad (11)$$

265 where $Q = CV$ is the charge present on the electrodes.

266 The DEG operation can be ideally partitioned into control cycles, each corresponding to a full
 267 oscillation between the flat equilibrium configuration and a maximally expanded
 268 configuration (that depends on the external excitation). In fact, DEG operation involves
 269 bidirectional electrical energy fluxes: in each cycle, an amount of electrical energy is initially
 270 spent by the external circuit to charge the DEG ($P_u < 0$), and a larger amount of electrical
 271 energy is successively recovered ($P_u > 0$) by progressively discharging the DEG. Several
 272 control strategies have been proposed for CD-DEGs employed as the PTO in OWCs,
 273 including prediction-less controls [18,19] and advanced controllers based on a statistical
 274 knowledge of the current sea state [33].

275

276 2.2.3. Air chamber model.

277 The U-OWC model and the CD-DEG model are coupled by means of the air pocket model.
 278 The latter relies on the air mass and energy conservation applied to the air volume in the
 279 chamber. In this regard, the equation presented in this section considers a general case in
 280 which the device is equipped with a system connecting the air chamber to the atmosphere,
 281 like a valve, so that a certain air flow rate \dot{m} (positive if air flows out of the chamber) is
 282 included in the computation. Air compressibility is accounted for by assuming that the
 283 thermodynamic process is isentropic [42,43]. In this context, the equation describing the air
 284 chamber dynamics is,

$$-\gamma(p + p_{atm}) \left(\frac{p + p_{atm}}{p_{atm}} \right)^{\frac{1}{\gamma}} \frac{\dot{m}}{\rho_{atm}} = \gamma \dot{\Omega}_a (p + p_{atm}) + \Omega_a \dot{p}, \quad (12)$$

where γ is the ratio of the specific heat at constant pressure and the specific heat at constant volume; ρ_{atm} is the atmospheric air density; p_{atm} is the atmospheric density; and Ω_a is the instantaneous air pocket volume. The calculation of Ω_a and its derivative leads to the following equations:

$$\Omega_a = b_2 b_3 \xi + \frac{\pi}{6} h_t (h_t^2 + 3e^2) N_D, \quad (13)$$

and

$$\dot{\Omega}_a = b_2 b_3 \dot{\xi} + \frac{\pi}{2} (h_t^2 + e^2) \dot{h}_t N_D. \quad (14)$$

If the chamber is equipped with a throttle valve, the air flow rate can be calculated through the equation

$$\dot{m} = C_v \pi \frac{d_v^2}{4} \sqrt{2 \rho_{atm} \left(\frac{p + p_{atm}}{p_{atm}} \right)^{1/\gamma} |p| \text{sign}(p)}, \quad (15)$$

where C_v is an empirical discharge coefficient, and d_v is the reference valve diameter.

3. In-field experimental validation.

This section presents the results of field experiments aimed at validating the proposed mathematical model of the coupled U-OWC/CD-DEG system. The experiments reported herein are the first examples of sea trials on an OWC with DEGs. At this stage, attention was restricted to the purely mechanical response of the system (regardless of electrical activation). In the following, a wide scope of the experimental activity is provided, and a comparison of experimental data and theoretical predictions is presented.

3.1. Set-up and data acquisition.

3.1.1 Experimental set-up

The experimental activity was carried out at the Natural Ocean Engineering Laboratory (NOEL) in Reggio Calabria (Italy). A U-OWC caisson is installed in a benign natural basin, where sea waves are generated naturally by the wind action. The U-OWC is incorporated in a metallic caisson connected to a vertical breakwater serving, in this context, as a ballast for the resulting system, while the CD-DEGs are installed on the ceiling of the air pocket (see Figure 3). The metallic caisson includes three independent chambers. Several identical CD-DEGs are installed on one of the lateral chambers, working simultaneously as shown in Figure 3.



Figure 3. Metallic caisson incorporating the U-OWC (a) with, on the top, four CD-DEGs on the lateral chamber (b). The U-OWC/CD-DEG is connected to a vertical breakwater serving as a ballast for the system. One of the CD-DEGs has been painted black to facilitate post-processing of the high-speed camera frames.

The chamber can house up to 4 CD-DEGs, though tests with a smaller number of DEGs can be performed closing the unused DEG housings with solid steel disks and seals. On top of the air chamber, a butterfly valve with nominal diameter of 100 mm is present, which is opened in the presence of rough sea states to limit the DEGs deformation.

CD-DEG prototypes have been manufactured using a commercial acrylic film, VHB 4905, produced by 3M. This material has been chosen as it features low mechanical rigidity and large extensibility, thus, it is adequate for deploying small-scale DEG prototypes [18]. Each DEG was built by overlapping and bonding together different layers of VHB 4905 so as to form a solid dielectric layer. The unstretched thickness of the resulting layer was of 4-5 mm with a diameter of 115 mm, while the final diameter, after pre-stretching by $\lambda_p = 3.4$ and installation on a rigid polycarbonate frame, was 390 mm.

In these tests, no electrodes were present on the CD-DEG prototypes, since no electrical activation was applied on the membranes and no power generation was pursued. In fact, the results of the tests were aimed at characterizing exclusively the mechanical response of the system.

An estimate of the power theoretically achievable with the considered CD-DEG samples (if electrical activation was applied) can be obtained based on constitutive models [19] and previous tests on CD-DEG samples made of VHB acrylic with carbon grease compliant electrodes [18,35]. According to those results, CD-DEGs can convert energy densities of 0.3-0.5 J/g per cycle. In the tests described here, the mass of dielectric material in each CD-DEG was about 40-50. Therefore, each of the employed CD-DEGs is potentially capable of power outputs of 10-25 W at an operating wave frequency of 0.4-0.5 Hz. Thus, equipping the device with four DEGs would give a theoretical rated power of 40-100 W.

Relevant measurements are obtained with ATM.ECO/N pressure transducers (PT) from STS. Specifically, one PT is installed at the inlet section of the collector, while three PTs are installed within the water column and one PT is installed in the air chamber as shows in Figure 4 (in the figure, the PT installed in the air chamber is not shown). The figure and Table 1 also show the relevant geometrical parameters.

Table 1. Geometrical characteristics of the U-OWC chamber equipped with CD-DEGs.

h_o [m]	d [m]	b_1 [m]	b_2 [m]	b_3 [m]	l_i [m]	h_c [m]	d_v [m]
0.57	1.9	0.5	1	1.23	0.8	1.9	0.10

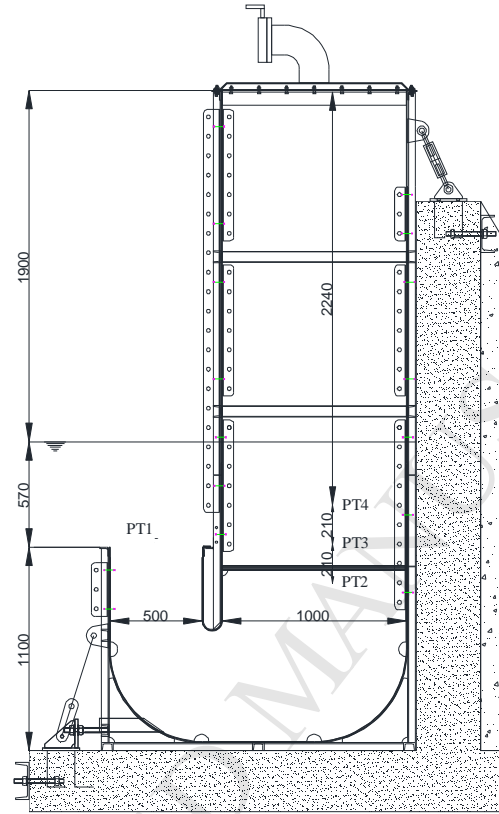


Figure 4. Vertical cross-section of the U-OWC and location of the pressure transducers (PT) in the water column. Lengths are in millimeters.

3.1.2 Data collection and post-processing

The PTs data were recorded with a sampling frequency of 10 Hz using a NI cDAQ-9174 acquisition board by National Instrument. The data were collected in short records representative of individual sea states. Specifically, each record was composed by 3000 samples, hence, each time series has a duration of 5 minutes, which is the typical time resolution of a sea state at the NOEL [44]. Globally, 102 sea states were collected, which are representative of different sea conditions, spanning from wind-generated seas to mixed sea

states. The corresponding significant wave height and peak spectral periods ranged in the intervals 0.15-0.45 m and 1.8-3.3 s.

The pressure data were used to simultaneously measure the excitation and the water column oscillation. In particular, the PT at the inlet section provides the wave pressure, Δp_w , cumulating the contribution due to diffracted and radiated waves, while the PTs in the water column and in the air chamber are used to measure, indirectly, the water column displacement. For this purpose, the method described by Boccotti et al. [45] and by Malara et al. [13] is employed. Specifically, given the simultaneous measurements of two PTs under water (e.g., the upper and the lower one) and of the PT in the air chamber, the water column acceleration ($\ddot{\xi}$) is calculated by the equation

$$\ddot{\xi} = g + \frac{p_u - p_l}{\rho \Delta z}, \quad (16)$$

where, p_l and p_u are the instantaneous pressures measured by the lower and the upper pressure transducers respectively, and Δz is their vertical distance. Then, the instantaneous displacement ξ is calculated by the equation

$$\xi = h_l - \frac{p_l - p}{\rho(g - \ddot{\xi})}, \quad (17)$$

h_l being the distance between the lower pressure transducer and the top of the U-OWC.

The deformation of one of the CD-DEGs was acquired by means of a high-speed camera (Point Grey GS3-U3-23S6M-C with lens 250F6C). The camera was placed at a distance of approximately 2 m from the DEGs, aligned with the top cover of the U-OWC collector (i.e., the equilibrium plane of the CD-DEGs). Data from the camera were synchronised with the PTs acquisitions through an external analogical trigger. Upwards deformations only were captured by the camera, as the membrane was hidden by the air chamber walls during its downward stroke. The acquired frames were then processed to obtain time-series of the CD-DEG tip elevation, h_t , using the procedure described by Moretti et al. [18]. Owing to the high sensitivity of the high-speed camera to fouling and humidity, measurement of the CD-DEGs

deformation was restricted to a few datasets. The effect of the DEGs on the system dynamics is however still measurable through the analysis of the time-series of ξ and p .

Examples of time-series of the different measured variables are reported in Figure 5, which shows a comparison of two tests featuring similar sea conditions, 4 CD-DEGs with $t_0 = 5$ mm, and two different aperture levels of the valve (closed and fully-open). In the presence of closed air chamber, the oscillations in p are larger (since no flow is practically exhausted through the valve), while oscillations in ξ are smaller. In effect, despite introducing a damping contribution in the water column dynamics, the valve aperture causes a reduction in the mechanical stiffness of the air chamber–DEGs system. The air pressure and the DEG tip displacement are in phase, since the electrically inactive DEG behaves as a purely elastic component (except for viscoelastic dissipative effects). For the same reason, p and h_t are in phase-opposition with ξ when the air chamber is closed, whereas some small phase-shifting is present when the valve is open (due to the air chamber dynamics introduced by the valve, described by Eq. (12)). Phase shifting among Δp_w and the other variables is always present, as a consequence of the water column dynamics (see Eq. (1)).

The oscillation amplitude of the CD-DEG monotonically increases with the air pressure, i.e., it is smaller when the valve is open (in spite of larger oscillations in ξ). This result suggests that a relief valve might be effectively employed as a safety device to protect the CD-DEGs in rough sea states.

A wider analysis of experimental results and comparison of different operating conditions is reported in [36], where the effect of the CD-DEGs on the U-OWC dynamics is investigated through a frequency-domain approach.

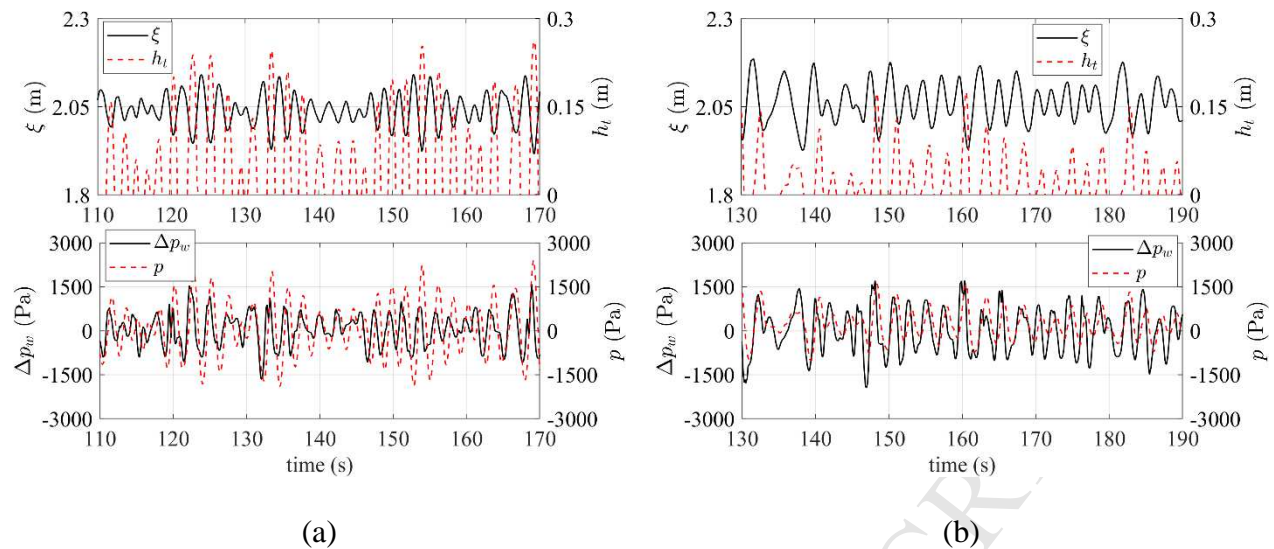


Figure 5. Time-series of water column displacement ξ , CD-DEG tip displacement h_t , wave pressure Δp_w , and air relative pressure p for two tests, in the presence of 4 CD-DEGs with $t_0 = 5$ mm. (a) Closed air chamber; (b) fully-open valve. Time-series of h_t are only relative to upwards membrane displacement, as the membrane was hidden by the collector walls during downward oscillations.

3.2. Model validation.

This section discusses a validation of the proposed U-OWC/CD-DEG coupled model. Attention is here restricted to the coupled dynamical response of the U-OWC and the DEGs. Therefore, attention is restricted to the following set of sub-models: the water column dynamics, the air chamber response, and the CD-DEG elastic model, excluding the radiation-diffraction problem and the effect of electrical activation. The latter sub-models have been validated in the past through purposed experiments [13,35] or against numerical models [46], and they might be further explored in the future through advanced tests including fully-functional DEGs and U-OWC nearfield sensing.

3.2.1. Model set-up and calibration.

The time domain dynamical model of the U-OWC with DEGs has been implemented in a Matlab & Simulink environment. The numerical model combines: the U-OWC dynamic equation (Eq. (1)), the dynamic equation of the air chamber with throttle valve (Eq. (12)) and the mechanical model of the CD-DEGs (Eq. (4), considering only the first term relative to the purely elastic response).

Simulations make use of the experimental datasets of the wave pressure Δp_w (i.e., the sum of the radiation and diffraction wave pressure) as the input. The simulation output consists of: the water column displacement, ξ , the air chamber pressure, p , and the CD-DEG tip displacement, h_t .

The parameters used in the U-OWC dynamic sub-model are the collector dimensions given in Table 1 and the hydraulic loss parameters. Based on previous tests on the reference U-OWC collector [13], the following loss parameters were used: $C_{dg} = 0.71$, $C_{in} = 0.13$.

The parameters in the CD-DEG elastic model are the Mooney-Rivlin coefficients, $C_{0,1}$, $C_{1,0}$. Based on available tests on the VHB material [18], the following values were considered: $C_{0,1} = 3700$ Pa, $C_{1,0} = 380$ Pa. For the air chamber model, atmospheric air density $\rho_{atm} = 1.2$ kg/m³ and adiabatic heat ratio $\gamma = 1.4$ were assumed.

The throttle valve has 10 positions, corresponding to different levels of aperture (from 100% open to fully-closed). In this experimental activity, in particular, five aperture levels were tested (including the fully open and closed states) that were sufficient for detecting clear alterations in the system dynamics associated with the throttle valve aperture level. The values of the discharge coefficient, C_v , corresponding to the aperture levels employed in the tests were identified through an experimental calibration procedure. Specifically, calibration tests were carried out with the valve mounted on the U-OWC collector, exploiting the air pressure variations induced by the water column oscillation. To isolate the contribution of the

valve, the DEGs were removed and replaced with undeformable disks. A set of acquisitions were performed, with the valve set to different positions. In each test, we measured the pressure p in the chamber and the level ξ of the water column. We then solved the dynamic equation of the air chamber (Eq. (12), with $h_t = 0$) for different values of C_v , using the measured time-series of ξ as the input, hence obtaining a set of time-series for p . We thus identified the value of C_v that minimizes the norm of the difference of experimental and model-based pressure time-series. Figure 6.a shows a comparison of experimental and theoretical time-series for a specific calibration test. Repeating this operation for each acquisition allowed the identification of a value of C_v for each of the relevant aperture levels used in the experiments, as shown in Figure 6.b. It should be noted that the discharge coefficient of the fully-closed valve is slightly larger than 0, as a result of the air leaks in the air chamber connections and in the valve. Moreover, over a given level of aperture (i.e., when the free flow passage area is rather wide), the value of C_v becomes practically constant.

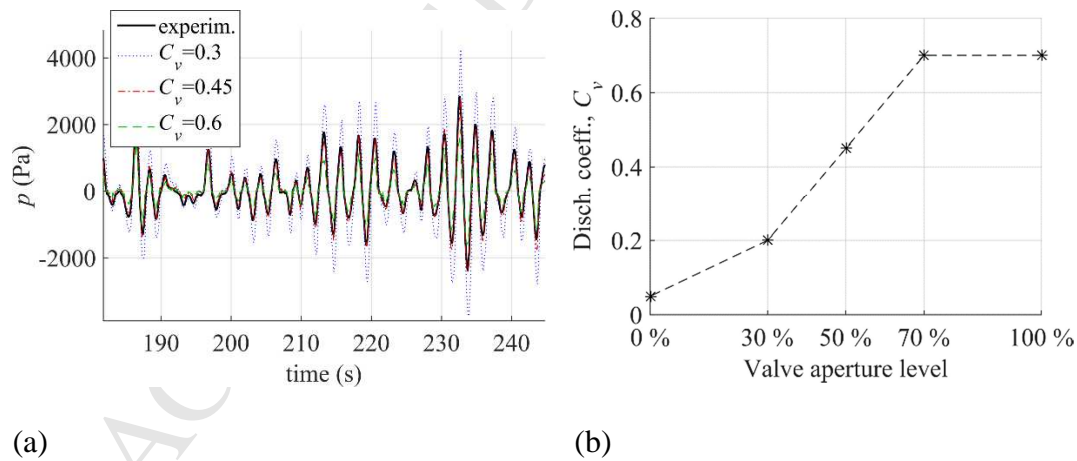


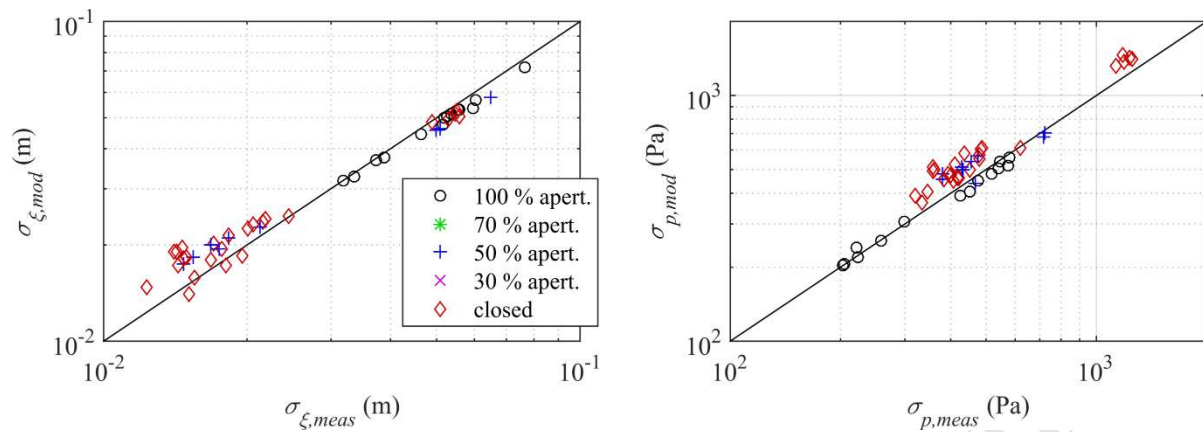
Figure 6. Discharge coefficient calibration: (a) comparison of the experimental air pressure time-series versus model-predicted time-series relative to different values of the discharge coefficient for a test with valve 50 % open; (b) Calibrated values of C_v at the different aperture levels of the valve used in the tests.

3.2.2. Comparison of model and experimental data.

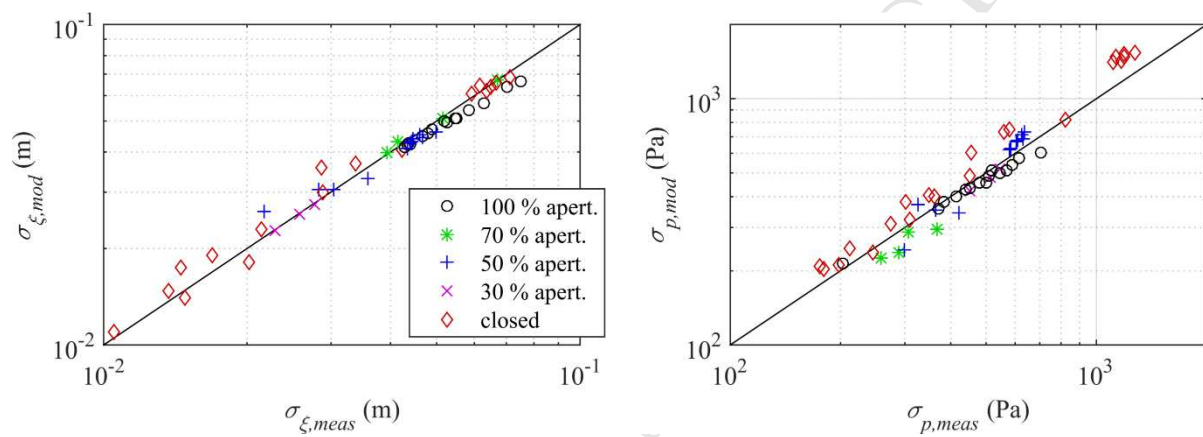
A set of simulations were run, using the approach described in Sect. 3.2.1. Each simulation aims at reproducing the U-OWC behaviour in a specific experimental dataset. Different records differ in terms of the following parameters (used as inputs in the simulations): measured pressure at the U-OWC inlet, number of DEGs in the chamber, DEGs thickness, discharge coefficient associated with the current valve position. An overview of the model performance against the different tests is provided in Figure 7, where we present vis-à-vis plots comparing the measured standard deviations of the water column displacement and the air chamber pressure ($\sigma_{\xi, meas}$ and $\sigma_{p, meas}$ respectively) and those obtained through the model ($\sigma_{\xi, mod}$, $\sigma_{p, mod}$). Direct comparison between modelled and experimental oscillation amplitude h_t of the CD-DEGs tip is, in contrast, omitted, as the tip height was measured only in a few tests and only during the outward stroke of the DEGs.

Figure 7.a shows results relative to the tests/simulations with 3 DEGs installed on the U-OWC chamber, while Figure 7.b is relative to the cases with 4 DEGs. In the plots, datasets relative to different aperture levels of the valve are denoted by different markers.

The plots show that, in average, tests with closed air chamber exhibit lower oscillation amplitude of ξ and larger oscillation amplitude in p than the corresponding tests with fully-open valve, as already observed in Sect. 3.1.2. Despite the broad variety of sea states and operating conditions characterising the various tests, the model is statistically capable of predicting the experimental behaviour rather effectively. In particular, data appear equally distributed above the bisector line of the vis-à-vis plots, thus confirming that the model does not provide any systematic overestimate (or underestimate) of the system oscillations.



(a) Tests with 3 DEGs



(b) Tests with 4 DEGs

Figure 7. Vis-à-vis comparison of experimental and model-predicted standard deviation of the time-series of the water column oscillations (left column) and the air chamber pressure (right column). Different markers refer to different levels of aperture of the valve. Plots (a) are relative with tests with 3 DEGs, plots (b) refer to tests with 4 DEGs.

Similarly to Malara et al. [13], in order to quantify the model error, for each dataset we define error metrics based on the time-series of ξ and p :

$$\varepsilon_{\xi} = \frac{\|\xi_{meas} - \xi_{mod}\|}{\sigma_{\xi,meas}}, \quad \varepsilon_p = \frac{\|p_{meas} - p_{mod}\|}{\sigma_{p,meas}} \quad (18)$$

where the subscript *meas* denotes the measured time-series whereas *mod* denotes model time-series, and operator $\|\cdot\|$ is the norm of the argument function. Errors relative to the different scenarios considered in Figure 7 (average over different datasets) are reported in Table 2.

Table 2. Estimate of the model error over the time-series of ξ and p .

	ε_{ξ}	ε_p
Tests with 3 DEGs	0.41	0.42
Tests with 4 DEGs	0.33	0.34
All tests	0.37	0.38

With reference to two datasets previously considered in Figure 5, for which measurements of the CD-DEG's tip height are also available, Figure 8 presents a comparison of experimental and theoretical time-series. In these tests, the model tends to overestimate the oscillation amplitudes of the different variables in the case of closed air chamber, and to underestimate them when the valve is open. The average errors over the considered portions of the datasets are as follow: $\varepsilon_{\xi}=0.39$ and $\varepsilon_p=0.50$ for the dataset shown in Fig. 8a (i.e., larger than the average values for the different tests considered in Table 2); $\varepsilon_{\xi}=0.22$ and $\varepsilon_p=0.21$ for the dataset shown in Fig. 8b (lower than the average error on the different tests). Despite the existing discrepancies, these results confirm a remarkable ability of the model to describe the trends and the dynamics of the relevant physical variables, including the CD-DEGs deformation. In particular, the possible presence of rather large errors in correspondence with

isolated oscillations does not affect the global agreement of the theoretical and experimental time-series on a statistical basis and the corresponding values of the average error.

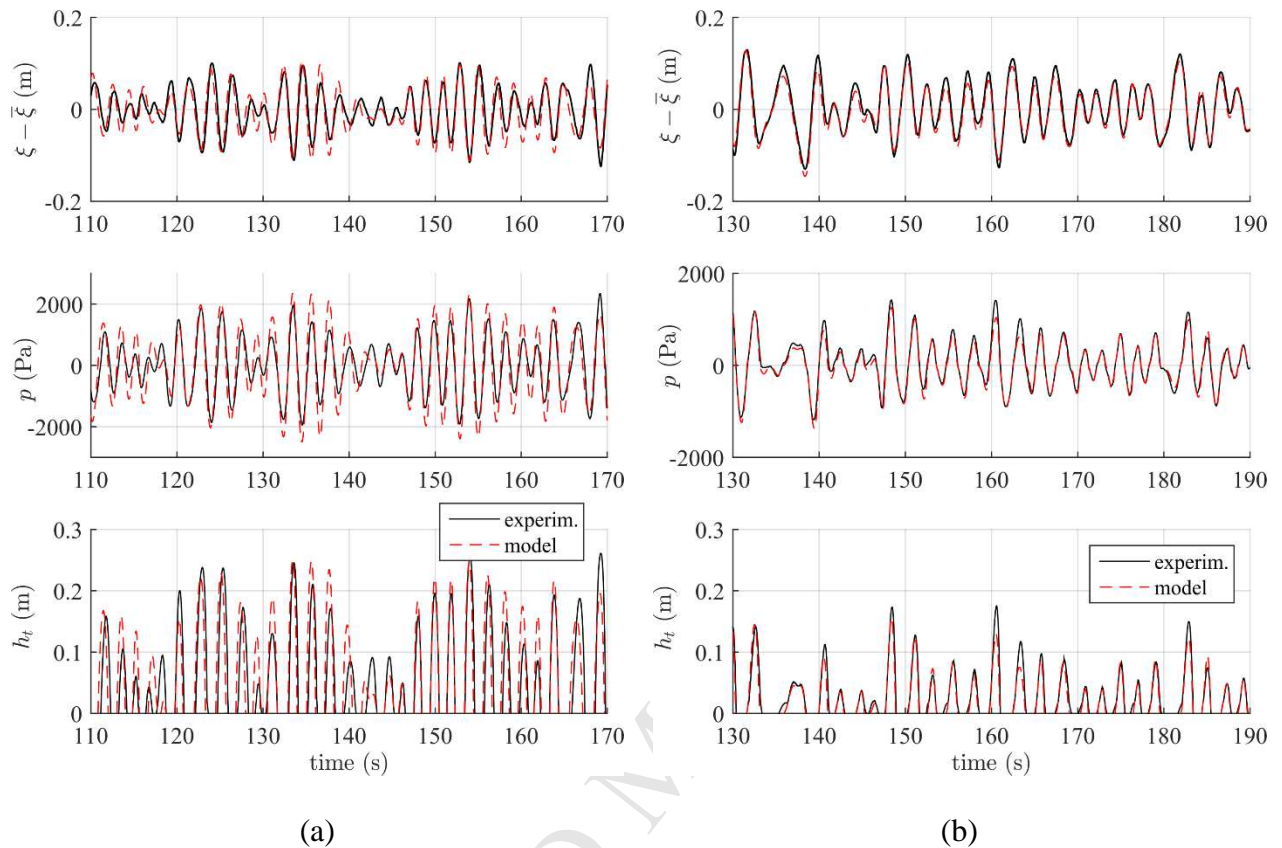


Figure 8. Comparison of model and experimental time-series of ξ (minus its mean value $\bar{\xi}$), p and h_t for two tests, in the presence of 4 CD-DEGs with $t_0 = 5$ mm. (a) Closed air chamber; (b) fully-open valve.

4. Analysis and simulation of a full-scale U-OWC with DEG PTO

Based on the proposed model, in this section we present a theoretical analysis of a full-scale application of a U-OWC equipped with a set of CD-DEGs as the PTO system.

In the analysis, reference is made to an existing U-OWC collector, installed in the port of Civitavecchia (Italy) [47,48]. The pilot wave farm in Civitavecchia is composed by a set of U-OWC chambers (with target power of 20 kW each) integrated on bottom-fixed breakwaters.

With the aim of evaluating the potential performance of DEG PTOs in full-scale applications, we hereby assume to replace the air turbine in one of the Civitavecchia U-OWC plant with a set of CD-DEGs. In this regard, reference is made to DEGs made of an optimised silicone material, specifically developed for DE application.

Silicone elastomers seem to be the most promising candidates for future DE applications. In effect, compared to other DEs, they bring a number of advantages, including: large potential for the improvement of electro-mechanical properties through the addition of compounds [49,50]; availability of manufacturing processes for high-quality films; and the possibility of manufacturing reliable dielectric-electrode stacks, by depositing carbon-charged silicone electrodes on the DE layers by blade casting, spray coating or screen printing [34,51].

4.1 Layout and assumptions

We consider a single U-OWC collector, the submerged part of which has the dimensions indicated in Table 3 [48]. The upper (out-of-water) portion of the collector is equipped with four CD-DEGs with the features listed in Table 3, installed on different (top and lateral) walls of the collector. The values of the hydraulic loss parameters for the Civitavecchia U-OWC chambers, provided in [15], are $C_{dg} = 0.46$, $C_{in} = 0.19$.

Table 3. Features of the considered full-scale U-OWC chamber with DEG PTO.

U-OWC dimensions		DEG PTO features		DE material properties	
h_o	2 m	N_D	4	Hyperelastic parameters	$C_{1,0} = 230$ kPa; $C_{0,1} = 0$
d	14.2 m	e	1.4 m	Dielectric constant	$\epsilon = 3.9 \cdot 8.85 \cdot 10^{-12}$ F/m
b_1	1.6 m	t_0	0.05 m	Rupture stretch	$\lambda_u = 8.8$
b_2	3.2 m	λ_p	1.3	Break-down electric field:	$E_0 = 100$ MV/m
b_3	3.87 m	n_l	80		$r_e = 1$
l_i	5 m			$E_{BD} = E_0 \lambda^{r_e}$	

The DEGs are made of a silicone material with the properties described by Madsen et al. [49]. This material is obtained blending a commercial silicone elastomer (ELASTOSIL LR3043/50) with a silicone oil (30 phr of LMS-152) so as to enhance the dielectric properties of the original elastomer while reducing its elastic stiffness. Although that material has been only investigated in the laboratory and is not a commercial product yet, we believe that it is representative of upcoming materials conceived for use as dielectric elastomer. The operating limits of the material are the ultimate rupture stretch, λ_u , expressing the maximum extensibility of the elastomer, and the maximum admissible value of the electric field, namely the break-down electric field, E_{BD} . Though in [49] the break-down field in the unstretched state only is measured (namely, 130 MV/m), based on literature results on different DEs [24], we assume that E_{BD} increases proportionally with the stretch λ to the power of r_e (see Table 3), with the value at unitary stretch conservatively taken equal to 100 MV/m. The considered silicone material is stiffer than the VHB acrylic considered in Sect. 3, therefore, the chosen pre-stretch is rather small. The total volume of DE material (over the 4 DEGs) is 0.74 m^3 . The number of layers, n_l , guarantees that the DEG output voltage is below 50 kV. The response of the U-OWC with DEG PTO is investigated in a set of typical sea states at the Civitavecchia site. The average wave climate at the installation site is characterized by sea states with JONSWAP spectral distribution [52] (standard peak enhancement factor of 3.3) whose peak period, T_p , and significant wave height, H_s , are correlated as follows [44]:

$$T_p = 8.5\pi\sqrt{H_s/(4g)}. \quad (19)$$

In order to assess the response of the device in rough sea conditions, significant wave heights of up to 5 m are considered.

574 4.2 CD-DEGs control

575 In this work, we make reference to a simple control strategy which does not require a-priori
576 knowledge of the incident waves, and only relies on the measured DEG deformations. Such a
577 strategy has been previously discussed in [19,33]. The operating cycle of a DEG is divided
578 into the following phases:

- 579 1) When the DEG expands from the flat configuration ($h_t = 0$) to an inflated
580 configuration (either inwards or outwards), no voltage is applied on its electrodes.
- 581 2) As the deformation (and capacitance) reaches a maximum, the DEG is rapidly
582 charged and its voltage is risen to the maximum value compatible with break-down.
583 During this phase (called priming), electrical energy is initially spent to charge the
584 DEG.
- 585 3) When the DEG moves back towards the flat position (i.e., its capacitance decreases),
586 the applied voltage is kept at the maximum value allowed by the break-down
587 condition. During this phase, the DEG outputs electrical power.
- 588 4) As the DEG reaches the flat position (minimum capacitance), it is fully discharged
589 and the stored energy is harvested.

590 In the simulations, the voltage rise during charging phase (1) and its decrease during
591 discharging phase (4) are simulated as quick first-order dynamics (with a characteristic time
592 much shorter than the full cycle duration).

593 Based on Eq. (10) and Table 3, the limiting condition for the voltage (applied during phase
594 3)) in relation to break-down is as follows:

$$595 \quad V \leq \frac{E_0 t_0}{n_l \lambda^{2-r_e}}. \quad (20)$$

596 Since the stretch λ is not uniform through the DEG (see Eq. (6)), the operating voltage during
597 phase 3) is obtained feeding the maximum stretch value (at the CD-DEG tip) into the right-
598 hand side of Eq. (20), namely

$$V = \frac{E_0 t_0}{n_l \lambda_t^{2-r_e}}, \quad (21)$$

where λ_t is the stretch calculated at the DEG tip (i.e., at $R = 0$).

601

602 4.3 Safety mode operation

603 We assume that the U-OWC air chamber is equipped with a safety valve with nominal
 604 diameter $d_v = 0.15$ m. Such a valve is closed in normal operating conditions, and it is partly
 605 opened in the presence of rough sea states to limit the CD-DEGs deformation. We assume
 606 that the level of aperture of the valve is adjusted on a mid-term basis, based on the knowledge
 607 of the average wave parameters (e.g., H_s or T_p).

608 Though, according to Madsen et al. [49], the maximum admissible stretch λ_u on the CD-
 609 DEGs is theoretically very large, we define a conservative threshold value, λ_{th} , that should
 610 not be surpassed but for a reduced amount of time. This measure is intended to increase the
 611 technical lifetime of the DE material, which, similarly to rubber, is expected to depend on the
 612 amplitude of the cyclic stretch variations to which it is subjected [53]. Here, we use $\lambda_{th} = 2$.

613 The level of aperture of the valve (i.e., the discharge coefficient C_v) in each sea state is
 614 chosen accordingly, so as to guarantee that the stretch does not surpass λ_{th} for more than 5%
 615 of the simulation time horizon. In statistical terms, this is equivalent to set an upper bound to
 616 the probability that the DEG deformation surpasses the chosen threshold.

617 In a real application, extensive analyses should be performed in order to choose meaningful
 618 values for λ_{th} and the corresponding limit percentage of occurrence. Such analyses should
 619 keep into account fatigue tests on the selected DE materials and should realize a compromise
 620 between an increase in DEG lifetime and a reduction in the energy production due to the
 621 stretch limitation. Moreover, dedicated analyses should be conducted in order to identify
 622 possible ageing effects due to electrical activation.

623

624 *4.4 Results and discussion*

625 The performance of the full-scale U-OWC has been simulated in a Matlab & Simulink
 626 environment. The U-OWC hydrodynamic parameters and the exciting pressure have been
 627 computed via the two-dimensional semi-analytical approach of Malara et al. [14]. The
 628 convolution integral involved in the computation of the radiation forces (see eq. (1)) has been
 629 approximated with a state-space model in order to reduce the computational burden [54]. In
 630 the simulations, different values of the emerged height h_c of the collector were considered.

631 Eight sea states with H_s between 1.5 and 5 m were considered. For each sea state, a
 632 simulation with a duration of 200 times the peak period was run, and the average power
 633 output was calculated from the DEG instantaneous power, P_u (see Eq. (11)). For the roughest
 634 sea states, in which aperture of the security valve is required, the calculation of the power
 635 output and the valve aperture was carried out through an iterative procedure. The iterative
 636 procedure was initiated by setting $C_v = 0$. Then, the coefficient was increased by steps of 0.1
 637 until the percentage occurrence of stretches larger than the threshold value λ_{th} was
 638 statistically reduced below 5%.

639 Simulation results are shown in Figure 9. The top plot shows the U-OWC power output for
 640 the different sea states (carrying increasing incident power). The central plot shows the
 641 percentage of the simulation time, $p_{\%}$, during which the DEGs stretch λ stays above the
 642 threshold λ_{th} . The bottom plot shows the minimum level of aperture of the security valve
 643 (expressed by C_v) required to keep $p_{\%} \leq 5\%$: $C_v = 0$ indicates that $p_{\%} \leq 5\%$ is achieved
 644 keeping the valve completely closed.

645

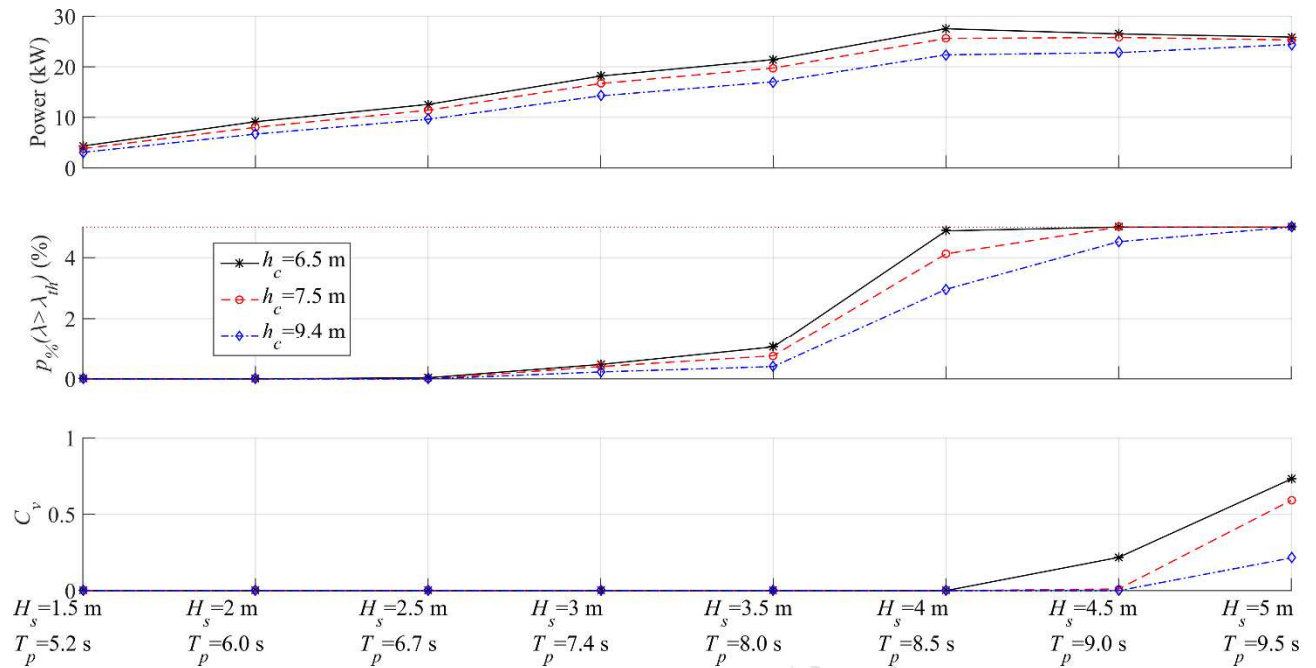


Figure 9. Response and performance of a full-scale U-OWC with DEG PTO in a set of reference sea states. Top plot: power output. Central plot: expected percentage of operating time during which the DEGs stretch surpasses the threshold value, λ_{th} . Bottom plot: Discharge coefficient expressing the required level of aperture of the security valve in the different sea states.

The proposed design of the DEG PTO results in a rated power output between 20 and 30 kW, consistently with simulation results relative to the scenario in which an air turbines is employed as the PTO [55]. For instance, a similar analysis conducted via Monte Carlo simulations was proposed by Malara and Arena [56], that provided power output estimations for four different turbine models (monoplane with/without guide vanes, biplane and contra-rotating). A comparison of the data produced in sea states with comparable significant wave height and peak period shows that the obtained converted powers are similar. A reduction in the air chamber height h_c (with respect to the nominal value of the Civitavecchia collectors, namely $h_c = 9.4$ m) results in an increase in the power output. Reducing h_c indeed causes a reduction in the air chamber compressibility, which in turn leads to larger DEG deformations.

In practice, the value of this design parameter should represent a compromise between the converter performance and safety requirements for the port infrastructure.

The trend of the power output is monotonically increasing with increasingly energetic sea states, up to $H_s = 4$ m. In rougher sea states, the power output experiments a saturation as a result of the partial aperture of the security valve. The required level of aperture of the valve increases with the incident wave power and with decreasing values of h_c . In practice, despite representing a limiting factor for the performance, an air chamber with large compressibility guarantees robustness in the presence of rough sea states, as it allows the achievement of a dramatic reduction in the DEGs deformation with relatively small diameters of the throttle valve. It is worth noticing that, in the mildest sea states, $p_{\%}$ is equal to 0 as the maximum deformation of the DEGs is permanently below the threshold value.

The presented results demonstrate that DEGs are a promising PTO solution for the U-OWC, as they potentially enable performance equal or better than that achievable with air turbines, despite their greater architectural simplicity. Moreover, simulation results suggest that safe plant operation can be achieved even in relatively rough sea states through the employment of a simple throttle valve.

5. Concluding remarks

This paper deals with the assessment of a U-oscillating water columns (U-OWCs) wave energy converter equipped with a dielectric elastomer generator (DEG) power take-off system. The mathematical model proposed in the paper has been obtained by combining a one-dimensional model based on the unsteady Bernoulli equation with an isentropic thermodynamic model for the air chamber dynamics, and a lumped-parameter electro-mechanical model of the DEG. The model reliability has been assessed against field data obtained from a small-scale experiment conducted in the NOEL (Natural Ocean Engineering

Laboratory) benign natural basin in Reggio Calabria (Italy). The presented experimental activity served as a first pilot investigation of a U-OWC with DEGs at sea. In this regard, the purely mechanical response of the system was investigated.

Based on the collected experimental data, it has been demonstrated that the model is able to capture the crucial features of the system dynamics in a variety of sea states, without systematic over- or under-estimations of the relevant physical parameters.

The validated model has been used for predicting the performance of a full-scale plant. For this purpose, the plant constructed in the port of Civitavecchia has been considered as a case study. The proposed mathematical model has been applied, assuming that one chamber of the plant is equipped with circular diaphragm DEGs (CD-DEGs) instead of turbines. Power output data have been obtained by running numerical simulations starting from spectrum compatible realizations of different sea states. It has been shown that a system integrating U-OWC and CD-DEGs may provide an average power output comparable to that of a U-OWC with turbines. Further, it has been shown that the presence of the CD-DEGs does not affect the reliability of the system, as the use of throttle valves prevents the inception of excessive pressures in severe sea states.

The results presented in this article pave the way for different future activities aimed at the advancement of the U-OWC with DEGs. The gathered data and numerical models will primarily allow the development of dry-run experiments aimed at evaluating control strategies and power output performance of DEG prototypes subject to loading histories similar to those recorded at sea. Furthermore, building upon the experience of this pilot activity, sea tests on DEG prototypes capable of actively extracting electrical power from the presented U-OWC plant will be carried out in the future.

711 **List of symbols**

712

Physical constants

<i>Symbol</i>	<i>Unit</i>	<i>Description</i>
g	m/s^2	Acceleration of gravity
p_{atm}	Pa	Atmospheric pressure
γ		Adiabatic exponent
ρ	kg/m^3	Sea water density
ρ_{atm}	kg/m^3	Atmospheric air density

U-OWC geometry and hydrodynamic model

<i>Symbol</i>	<i>Unit</i>	<i>Description</i>
b_1	m	Width of the U-duct
b_2	m	Width of the main collector
b_3	m	Transversal width of the collector
h_o	m	Depth of the collector inlet section
l_i	m	Length of the U-duct
$C(\xi, \xi)$	s	Time-dependent damping coefficient
C_{dg}, C_{in}		Head loss coefficients
$H(\infty)$	m	Infinite frequency added head
H_s	m	Significant wave height
$K(\tau)$	m/s^2	Radiation convolution kernel
$M(\xi)$	s^2	Time-dependent Inertial coefficient
R_{h1}, R_{h2}	m	Hydraulic radii of the U-duct
T_p	s	Wave peak period
ξ	m	Distance of the air chamber top wall from the free surface
τ	s	Time coordinate

$\Delta p^{(D)}$	Pa	Wave pressure in a diffractive wave field
CD-DEG geometry and model		
<i>Symbol</i>	<i>Unit</i>	<i>Description</i>
e	m	Radius (flat pre-stretched configuration)
e_0	m	Radius before pre-stretch
h_t	m	Tip element displacement
n_l		Number of layers
r_e		Exponential parameter for the break-down electric field expression
t	m	Local thickness
t_0	m	Thickness before pre-stretch
C	F	Capacitance
$C_{1,0}, C_{0,1}$	Pa	Mooney-Rivlin hyperelastic parameters
E	V/m	Local electric field
E_0	V/m	Break-down electric field at unitary stretch
E_{BD}	V/m	Break-down electric field
P_u	W	Instantaneous electrical power output
Q	C	charge
R	m	Radial coordinate on the unstretched CD-DEG
U_m	J	Total elastic energy
V	V	Voltage
ϵ	F/m	DE's dielectric constant
λ		Local stretch
λ_p		Pre-stretch
Ψ	J/m ³	Strain-energy density function
Ω_c	m ³	CD-DEG cap subtended volume

Air chamber geometry and model

<i>Symbol</i>	<i>Unit</i>	<i>Description</i>
d_v	m	Valve reference diameter
h_c	m	Air chamber height
\dot{m}	kg/s	Mass flow rate through the apertures
p	Pa	Air chamber gauge pressure
C_v		Valve discharge coefficient
N_D		Number of CD-DEGs on the air chamber
Ω_a	m ³	Instantaneous air pocket volume

Experiments and simulations parameters

<i>Symbol</i>	<i>Unit</i>	<i>Description</i>
h_l	m	Distance between the lower pressure transducer and the air chamber top wall
p_l, p_u	Pa	Pressure measured by the submerged transducers
$p_{\%}$	%	Maximum percentage time (on the simulation horizon) during which the stretch λ is allowed to be larger than λ_{th}
$\varepsilon_p, \varepsilon_{\xi}$		Errors in the simulated air pressure and water column displacement compared to the experimental data (average over a dataset)
λ_{th}		Threshold safety value for the DEG stretch
$\sigma_{p, meas}$	Pa	Measured standard deviation of the air pressure
$\sigma_{\xi, meas}$	m	Measured standard deviation of the water column displacement
Δz	m	Distance between the submerged transducers

Operators and notation

<i>Symbol</i>	<i>Description</i>
$\dot{\varphi}$	Differentiation with respect to time of a generic variable φ
$\bar{\varphi}$	Time averaged value of a generic variable φ
$\text{sign}(\varphi)$	Sign of a generic variable φ

Acknowledgement

Malara, Scialò, Romolo and Arena acknowledge “Regione Calabria, Dipartimento 2 - Presidenza Settore 3 – Ricerca scientifica e Innovazione tecnologica” supporting the activities of the project “GRE.ENE.LOG.” (CUP J38C17000170006) by the funding scheme “POR CALABRIA FESR 2014 2020 - Azione 1.2.2 ‘Supporto alla realizzazione di progetti complessi di attività di ricerca e sviluppo su poche aree tematiche di rilievo e all’applicazione di soluzioni tecnologiche funzionali alla realizzazione delle strategie di S3’ ”.

Moretti, Daniele, Vertechy and Fontana acknowledge the support from "Regione Toscana" (Italy) under the project EOLO (FAR FAS 2014-A).

References

- [1] A.F.O. Falcão, J.C.C. Henriques, Oscillating-water-column wave energy converters and air turbines: A review, *Renew. Energy*. 85 (2016) 1391–1424. doi:10.1016/j.renene.2015.07.086.
- [2] T. V. Heath, A review of oscillating water columns, *Philos. Trans. R. Soc. A Math. Phys. Eng. Sci.* 370 (2012) 235–245. doi:10.1098/rsta.2011.0164.
- [3] A.F.O. Falcão, L.M.C. Gato, 8.05 - Air Turbines, in: *Compr. Renew. Energy*, Elsevier, Oxford, 2012: pp. 111–149. doi:http://dx.doi.org/10.1016/B978-0-08-087872-0.00805-2.
- [4] A.F.O. Falcão, J.C.C. Henriques, L.M.C. Gato, R.P.F. Gomes, Air turbine choice and optimization for floating oscillating-water-column wave energy converter, *Ocean Eng.* 75 (2014) 148–156. doi:10.1016/J.OCEANENG.2013.10.019.
- [5] A.F. de O. Falcão, The shoreline OWC wave power plant at the Azores, in: *Proc. 4th Eur. Wave Energy Conf.*, Aalborg, Denmark, 2000: pp. 42–48.
- [6] T.J.T. Whittaker, D. Langston, N. Fletcher, M. Shaw, A.F. de O. Falcão, Islay

LIMPET wave power plant, Belfast, 2002.

- [7] G. Ibarra-Berastegi, J. Sáenz, A. Ulazia, P. Serras, G. Esnaola, C. Garcia-Soto, Electricity production, capacity factor, and plant efficiency index at the Mutriku wave farm (2014–2016), *Ocean Eng.* 147 (2018) 20–29. doi:10.1016/j.oceaneng.2017.10.018.
- [8] R.P.F. Gomes, J.C.C. Henriques, L.M.C. Gato, A.F.O. Falcão, Hydrodynamic optimization of an axisymmetric floating oscillating water column for wave energy conversion, *Renew. Energy*. 44 (2012) 328–339. doi:10.1016/j.renene.2012.01.105.
- [9] L. Martinelli, P. Pezzutto, P. Ruol, Experimentally based model to size the geometry of a new OWC device, with reference to the mediterranean sea wave environment, *Energies*. 6 (2013) 4696–4720. doi:10.3390/en6094696.
- [10] P. Boccotti, On a new wave energy absorber, *Ocean Eng.* 30 (2003) 1191–1200. doi:10.1016/S0029-8018(02)00102-6.
- [11] P. Boccotti, Comparison between a U-OWC and a conventional OWC, *Ocean Eng.* 34 (2007) 799–805. doi:10.1016/j.oceaneng.2006.04.005.
- [12] F. Arena, A. Romolo, G. Malara, V. Fiamma, V. Laface, The first worldwide application at full-scale of the REWEC3 device in the Port of Civitavecchia: Initial energetic performances, in: *Prog. Renew. Energies Offshore - Proc. 2nd Int. Conf. Renew. Energies Offshore, RENEW 2016*, 2016.
- [13] G. Malara, A. Romolo, V. Fiamma, F. Arena, On the modelling of water column oscillations in U-OWC energy harvesters, *Renew. Energy*. 101 (2017) 964–972. doi:10.1016/j.renene.2016.09.051.
- [14] G. Malara, R.P.F. Gomes, F. Arena, J.C.C. Henriques, L.M.C. Gato, A.F.O. Falcão, The influence of three-dimensional effects on the performance of U-type oscillating water column wave energy harvesters, *Renew. Energy*. 111 (2017) 506–522.

doi:10.1016/j.renene.2017.04.038.

- [15] F. Arena, A. Romolo, G. Malara, V. Fiamma, V. Laface, Validation of the U-Oscillating Water Column model by full-scale experimental data, in: Proc. 12th Eur. Wave Tidal Energy Conf., Cork, Ireland, 2017.
- [16] G. Malara, F. Arena, Response of U-Oscillating Water Column arrays: semi-analytical approach and numerical results, *Renew. Energy*. 138 (2019) 1152–1165.
doi:10.1016/j.renene.2019.02.018.
- [17] A.F.O. Falcão, L.M.C. Gato, J.C.C. Henriques, J.E. Borges, B. Pereiras, F. Castro, A novel twin-rotor radial-inflow air turbine for oscillating-water-column wave energy converters, *Energy*. 93 (2015) 2116–2125. doi:10.1016/J.ENERGY.2015.10.046.
- [18] G. Moretti, G. Pietro Rosati Papini, M. Righi, D. Forehand, D. Ingram, R. Vertechy, M. Fontana, Resonant wave energy harvester based on dielectric elastomer generator, *Smart Mater. Struct.* 27 (2018) 35015. doi:10.1088/1361-665X/aaab1e.
- [19] R. Vertechy, G.P. Rosati Papini, M. Fontana, G. Pietro Papini Rosati, M. Fontana, G.P. Rosati Papini, M. Fontana, Reduced Model and Application of Inflating Circular Diaphragm Dielectric Elastomer Generators for Wave Energy Harvesting, *J. Vib. Acoust.* 137 (2014) 011016. doi:10.1115/1.4028508.
- [20] F. Carpi, D. De Rossi, R. Kornbluh, R.R.E. Pelrine, P. Sommer-Larsen, *Dielectric Elastomers as Electromechanical Transducers: Fundamentals, Materials, Devices, Models and Applications of an Emerging Electroactive Polymer Technology*, Elsevier Science, Amsterdam, The Netherlands, 2011. doi:10.1016/B978-0-08-047488-5.X0001-9.
- [21] R. Pelrine, R. Kornbluh, Q. Pei, J. Joseph, High-Speed Electrically Actuated Elastomers with Strain Greater Than 100 %, *Science* (80-.). 287 (2000) 836–840.
doi:10.1126/science.287.5454.836.

- 789 [22] G. Thomson, D. Yurchenko, D.V. Val, Dielectric Elastomers for Energy Harvesting,
790 in: R. Manyala (Ed.), *Energy Harvest.*, IntechOpen, 2018: pp. 41–61.
791 doi:10.5772/intechopen.74136.
- 792 [23] E. Bortot, M. Gei, Harvesting energy with load-driven dielectric elastomer annular
793 membranes deforming out-of-plane, *Extrem. Mech. Lett.* 5 (2015) 62–73.
794 doi:10.1016/J.EML.2015.09.009.
- 795 [24] R. Kaltseis, C. Keplinger, S.J. Adrian Koh, R. Baumgartner, Y.F. Goh, W.H. Ng, A.
796 Kogler, A. Tröls, C.C. Foo, Z. Suo, S. Bauer, Natural rubber for sustainable high-
797 power electrical energy generation, *RSC Adv.* 4 (2014) 27905–27913.
798 doi:10.1039/c4ra03090g.
- 799 [25] R.D. Kornbluh, R. Pelrine, H. Prahla, A. Wong-Foy, B. McCoy, S. Kim, J. Eckerle,
800 T. Low, From boots to buoys: Promises and challenges of dielectric elastomer energy
801 harvesting, *Electroact. Polym. Mater.* 9781461408 (2012) 67–93. doi:10.1007/978-1-
802 4614-0878-9_3.
- 803 [26] S. Shian, J. Huang, S. Zhu, D.R. Clarke, Optimizing the Electrical Energy Conversion
804 Cycle of Dielectric Elastomer Generators, *Adv. Mater.* 26 (2014) 6617–6621.
805 doi:10.1002/adma.201402291.
- 806 [27] R. Pelrine, R. Kornbluh, J. Eckerle, P. Jeuck, S. Oh, Q. Pei, S. Stanford, Dielectric
807 elastomers: Generator mode fundamentals and applications, *Proc. SPIE* 4329, *Smart*
808 *Struct. Mater.* 42 (2001) 148–156.
- 809 [28] S.J.A. Koh, C. Keplinger, T. Li, S. Bauer, Z. Suo, Dielectric elastomer generators:
810 How much energy can be converted?, *IEEE/ASME Trans. Mechatronics.* 16 (2011)
811 33–41. doi:10.1109/TMECH.2010.2089635.
- 812 [29] S. Chiba, M. Waki, K. Fujita, K. Masuda, T. Ikoma, Simple and Robust Direct Drive
813 Wave Power Generation System Using Dielectric Elastomers, *J. Mater. Sci. Eng. B.* 7

- (2017) 1–2. doi:10.17265/2161-6221/2017.1-2.005.
- [30] S. Chiba, M. Waki, T. Wada, Y. Hirakawa, K. Masuda, T. Ikoma, Consistent ocean wave energy harvesting using electroactive polymer (dielectric elastomer) artificial muscle generators, *Appl. Energy*. 104 (2013) 497–502. doi:10.1016/j.apenergy.2012.10.052.
- [31] G. Moretti, M. Fontana, R. Vertechy, Model-based design and optimization of a dielectric elastomer power take-off for oscillating wave surge energy converters, *Meccanica*. 50 (2015) 2797–2813. doi:10.1007/s11012-015-0235-8.
- [32] A. Babarit, J. Singh, C. Mélis, A. Watez, P. Jean, A linear numerical model for analysing the hydroelastic response of a flexible electroactive wave energy converter, *J. Fluids Struct.* 74 (2017) 356–384. doi:10.1016/j.jfluidstructs.2017.06.003.
- [33] G.P. Rosati Papini, G. Moretti, R. Vertechy, M. Fontana, Control of an oscillating water column wave energy converter based on dielectric elastomer generator, *Nonlinear Dyn.* 92 (2018) 181–202. doi:10.1007/s11071-018-4048-x.
- [34] G. Moretti, M. Righi, R. Vertechy, M. Fontana, Fabrication and test of an inflated circular diaphragm dielectric elastomer generator based on PDMS rubber composite, *Polymers (Basel)*. 9 (2017) 283. doi:10.3390/polym9070283.
- [35] G. Moretti, G. Pietro Rosati Papini, L. Daniele, D. Forehand, D. Ingram, R. Vertechy, M. Fontana, Modelling and testing of a wave energy converter based on dielectric elastomer generators, *Proc. R. Soc. A Math. Phys. Eng. Sci.* 475 (2019) 20180566. doi:10.1098/rspa.2018.0566.
- [36] F. Arena, L. Daniele, V. Fiamma, M. Fontana, G. Malara, G. Moretti, A. Romolo, G.P. Rosati Papini, A. Scialò, R. Vertechy, Field experiments on dielectric elastomer generators integrated on a U-OWC wave energy converter, in: *Proc. 37th Int. Conf. Ocean. Offshore Arct. Eng., ASME, Madrid, Spain, 2018.*

- [37] S. Rosset, H.R. Shea, Flexible and stretchable electrodes for dielectric elastomer actuators, *Appl. Phys. A*. 110 (2013) 281–307. doi:10.1007/s00339-012-7402-8.
- [38] W.E. Cummins, The impulse response function and ship motions, *Schiffstechnik* (1962). 57 (1962) 101–109. doi:10.1179/2056711115Y.000000000001.
- [39] C.C. Mei, M. Stiassnie, D.K.K. Yue, Theory and applications of ocean surface waves, World Scientific, Singapore, 2005.
- [40] G. Holzapfel, Nonlinear solid mechanics: A continuum approach for engineering, Wiley, 2000. doi:10.1023/A:1020843529530.
- [41] L. Dorfmann, R.W. Ogden, Nonlinear theory of electroelastic and magnetoelastic interactions, Springer US, 2014. doi:10.1007/978-1-4614-9596-3.
- [42] A.J.N.A. Sarmiento, A.F. de O. Falcão, Wave generation by an oscillating surface-pressure and its application in wave-energy extraction, *J. Fluid Mech.* 150 (1985) 467–485. doi:10.1017/S0022112085000234.
- [43] A.F. de O. Falcão, P.A.P. Justino, OWC wave energy devices with air flow control, *Ocean Eng.* 26 (1999) 1275–1295. doi:10.1016/S0029-8018(98)00075-4.
- [44] P. Boccotti, Chapter 3 - Random Wind-Generated Waves: Basic Concepts, in: *Wave Mech. Wave Loads Mar. Struct.*, Butterworth-Heinemann, Oxford, 2015: pp. 43–61. doi:https://doi.org/10.1016/B978-0-12-800343-5.00003-2.
- [45] P. Boccotti, P. Filianoti, V. Fiamma, F. Arena, Caisson breakwaters embodying an OWC with a small opening-Part II: A small-scale field experiment, *Ocean Eng.* 34 (2007) 820–841. doi:10.1016/j.oceaneng.2006.04.016.
- [46] G. Malara, R.P.F. Gomes, F. Arena, J.C.C. Henriques, L.M.C. Gato, A.F.O. Falcão, Hydrodynamic characteristics of a U-OWC plant : comparison between analytical and numerical results, in: *Proc. 11th Eur. Wave Tidal Energy Conf.*, Nantes, France, 2015: pp. 1–10.

- 864 [47] F. Arena, A. Romolo, G. Malara, A. Ascanelli, On Design and Building of a U-OWC
 865 Wave Energy Converter in the Mediterranean Sea: A Case Study, in: Proc. 32nd Int.
 866 Conf. Ocean. Offshore Arct. Eng., 2013: p. V008T09A102. doi:10.1115/omae2013-
 867 11593.
- 868 [48] F.M. Strati, G. Malara, F. Arena, Performance optimization of a U-Oscillating-Water-
 869 Column wave energy harvester, *Renew. Energy*. 99 (2016) 1019–1028.
 870 doi:10.1016/j.renene.2016.07.080.
- 871 [49] F.B. Madsen, L. Yu, P. Mazurek, A.L. Skov, A simple method for reducing inevitable
 872 dielectric loss in high-permittivity dielectric elastomers, *Smart Mater. Struct.* 25
 873 (2016) 75018. doi:10.1088/0964-1726/25/7/075018.
- 874 [50] P. Caspari, S.J. Dünki, F.A. Nüesch, D.M. Opris, Dielectric elastomer actuators with
 875 increased dielectric permittivity and low leakage current capable of suppressing
 876 electromechanical instability, *J. Mater. Chem. C*. 6 (2018) 2043–2053.
 877 doi:10.1039/c7tc05562e.
- 878 [51] B. Fasolt, M. Hodgins, G. Rizzello, S. Seelecke, Effect of screen printing parameters
 879 on sensor and actuator performance of dielectric elastomer (DE) membranes, *Sensors*
 880 *Actuators A Phys.* 265 (2017) 10–19. doi:10.1016/J.SNA.2017.08.028.
- 881 [52] K. Hasselmann, T.P. Barnett, E. Bouws, H. Carlson, D.E. Cartwright, K. Enke, J.A.
 882 Ewing, H. Gienapp, D.E. Hasselmann, P. Kruseman, A. Meerburg, P. Muller, D.J.
 883 Olbers, K. Richter, W. Sell, H. Walden, Measurements of Wind-Wave Growth and
 884 Swell Decay during the Joint North Sea Wave Project (JONSWAP), *Ergnzungsh. Zur*
 885 *Dtsch. Hydrogr. Zeitschrift R. A*(8) (1973) p.95.
- 886 [53] P.Y. Le Gac, M. Arhant, P. Davies, A. Muhr, Fatigue behavior of natural rubber in
 887 marine environment: Comparison between air and sea water, *Mater. Des.* 65 (2015)
 888 462–467. doi:10.1016/j.matdes.2014.09.032.

- 889 [54] Z. Yu, J. Falnes, State-space modelling of a vertical cylinder in heave, Appl. Ocean
890 Res. 17 (1995) 265–275. doi:10.1016/0141-1187(96)00002-8.
- 891 [55] F. Arena, G. Malara, A. Romolo, A U-OWC wave energy converter in the
892 Mediterranean Sea: Preliminary results on the monitoring system of the first prototype,
893 in: Guedes Soares (Ed.), Proc. 1st Int. Conf. Renew. Energies Offshore -
894 RENEW2014, CRC Press, Lisbon, Portugal, 2014: pp. 417–421. doi:10.1201/b18973-
895 59.
- 896 [56] G. Malara, F. Arena, Analytical modelling of an U-Oscillating Water Column and
897 performance in random waves, Renew. Energy. 60 (2013) 116–126.
898 doi:10.1016/j.renene.2013.04.016.

899

900

901

- Model of a U-shaped oscillating water column with dielectric elastomer generator
- Tests on a scaled prototype are carried out in a benign sea basin
- Good agreement of model prediction and experimental data over a wide set of tests
- The model is used to predict the performance of a full-scale U-OWC with DEG
- First step toward the demonstration of the feasibility of dielectric elastomer WEC